Surface gravity waves at equilibrium with a steady wind

Roman E. Glazman

Jet Propulsion Laboratory, California Institute of Technology, Pasadena, CA 91009

ABSTRACT

Observations of wave fields' spatial evolution and of gravity wave spectra $S(\omega)$ under

1. Introduction

One of the outstanding issues in dynamics of the upper ocean is the physical mechanism through which the energy and momentum are transferred from wind to various components of ocean circulation. Air-sea interaction involves generation of surface gravity waves which may play an important role in air-sea exchanges on larger scales. The present, primarily experimental, study is focused on weakly nonlinear wave-wave interactions and wave dispersion as possible factors of energy and momentum exchanges between the wave field and larger-scale oceanic motions. In particular we shall stress that, at a sufficiently high degree of sea development - characteristic to open ocean waves, the regime of air-sea interaction is markedly different from that observed for a poorly developed sea state in which the wave energy is dissipated locally.

In general, dissipation of the wave energy can occur through a variety of mechanisms effective in different spectral bands. However, the main dissipation mechanism currently assumed in most wave studies and in wave models is due to the breaking of short gravity waves. The source functions parametrizing this mechanism are essentially empirical. The same is true with respect to the wind input source function. One particular requirement used in wave models' design is the convergence to the fully developed sea (FDS) at the

spectrum, while appropriate under certain specific conditions, does not represent any fundamental limit on the wave evolution process.

Our conclusions are based on analysis of wave observations unde carefully selected cases characterized by relatively simple wave g which can be described using idealized dynamical models. This all much as possible various adjustable parameters and empirical sour with wave spectra we analyzed spatial evolution of wave fields alon understand the role of the wave field inhomogeneity. Owning to t of tetrad wave-wave interactions, the characteristic spatial scale evolution is of order of a hundred kilometers. Therefore, experi processes addressed in the present work cannot be conducted in w other confined basins. Moreover, being interested in deep-water gra make sure that the characteristic depth is at least of the order of length. The latter, as our data show, attains a few hundred meters.

The background information on equilibrium wave spectra is re and experimental data are presented in section 3. In sections 4 interpreted, and conclusions are summarized in section 7.

2. Basic relations for developed sea spectra: an overview

The wave age, ξ, is defined as the ratio of the phase velo corresponding to the spectral peak frequency ω_0 to the mean wind (e.g., at 10 m height):

$$\xi = C_0/U \qquad (= g/U\omega_0)$$

The data presented in section 3 cover a broad range of sea developme of moderate degree $\xi \sim O(1)$ to a very well developed sea $\xi \gg 1$. This in the framework of the weak turbulence theory (WTT) for sur [Zakharov and Filonenko, 1966; Zakharov and Zaslavskii, 1982-19 for wave-wave interaction in resonant wave tetrads [Hasselma summarize a few relevant concepts which facilitate the interpretation

For a statistically stationary and spatially homogeneous wave fiel possible regimes of wave energy and action flow through the spectru cascade in which the wave energy flux, Q, is conserved and the inver the wave action flux, P, is conserved [Zakharov and Filonenko, 1 Zaslavskii, 1982] while the energy flux is zero. In the course of the w the inverse cascade of the wave action is accompanied by a non-c energy to low wavenumbers [Hasselmann, 1962; Hasselmann et al.,

cascade causes a gradual decrease of the spectral peak wavenumber, k_0, with an increasing wind fetch (distance along the wind vector) and duration (time from the start of the wind). Thus, at a given wind U, the non-dimensional spectral peak frequency $\tilde{\omega}_0 = U\omega_0/g$ represents a measure of wave development. In the present work, we consider only the cases with an infinite wind duration. Hence, the degree of sea development depends only on the wind fetch, and the wave field is spatially inhomogeneous. Kolmogorov-type spectra can still be used in this situation for crude estimates - as demonstrated by Zakharov and Zaslavskii [1983] and Glazman and Srokosz [1991] - although certain refinements, as discussed in the following sections, are necessary.

For moderately developed waves ($\xi \leq 1$), the relative extent of the wavenumber subrange corresponding to the inverse cascade is negligible compared to that of the direct cascade. Then the "equilibrium" range in the (energy) spectrum is dominated by [Zakharov and Filonenko, 1966]:

$$F(k) = \alpha_q g^{-1/2} Q^{1/3} k^{-7/2}, \quad (\quad S(\omega) = 2\alpha_q g Q^{1/3} \omega^{-4}) \tag{2.2}$$

where F(k) is the wavenumber spectrum and S(ω) is the frequency spectrum. The non-dimensional constant α_q plays a role similar to that of the Kolmogorov constant in turbulence. Q is the spectral flux of energy toward high wavenumbers. In a statistically anisotropic wave field, the two-dimensional wavenumber spectrum includes an angular distribution factor $\Psi_1(\theta)$, which is assumed here to be normalized to yield unity upon

for a spatially homogeneous wave field - yields a Kolmogorov spectrum determined by the inverse conservative cascade of wave action:

$$F(k) = \alpha_p P^{1/3} k^{-10/3} \tag{2.3}$$

This corresponds to $S(\omega) \sim \omega^{-11/3}$.

One can further idealize the situation by assuming that the wind energy input is concentrated at wavenumbers (the "generation range") separating these two inertial subranges. As discussed in the following sections, the forms (2.2) and (2.3) are not very useful, for we do not know in advance how the input fluxes, Q_u and P_u, are related to the inertial fluxes Q and P through the spectrum. On dimensional grounds, P and Q can be expressed in terms of the mean wind speed U as:

$$P \propto g^{-2}U^4 \ , \qquad Q \propto U^3 \tag{2.4}$$

Then, the entire equilibrium range can be presented in the form

$$F(k) = \beta(U^2/g)^{2\mu} k^{-4+2\mu} \ , \qquad S(\omega) = 2\beta g^2(U/g)^{4\mu}\omega^{-5+4\mu} \tag{2.5}$$

which reduces to (2.2) or (2.3) by setting $\mu=1/4$ or $\mu=1/3$ for $\xi \leq 1$ and $\xi >> 1$, respectively. Furthermore, β is the generalized Phillips constant whose value can be expressed in terms of the Kolmogorov constants. In general, μ is a slowly decreasing function of the wavenumber [Glazman et al., 1988; Glazman and Weichman, 1989; Glazman and Srokosz, 1991]: $\mu=\mu(k)$, Fig. 1. Its maximum lies in the subrange associated with the inverse cascade. At frequencies above the generation range, μ passes through 1/4 and reaches zero in the Phillips "saturation" range [Phillips, 1977] (if the energy input is sufficiently high for such a range to occur). In the Phillips range the spectrum tends to:

$$F(k) = \beta k^{-4} \tag{2.6}$$

This corresponds to a non-Gaussian field of the surface height variation characterized by cusped wave crests. WTT is not applicable to the strongly nonlinear waves described by (2.6). The drop of μ below 1/4 (i.e. from weak turbulence to stronger nonlinearity) can be described based on a heuristic theory of multi-wave interactions [Glazman, 1992].

Experimentalists usually report an overall apparent value of the exponent and a wave-age-dependent value of the Phillips constant β in the power laws (2.5). This "effective"

exponent yields an apparent fractal (Hausdorff) dimension of the surface: $D_H=2+\mu$ [Glazman and Weichman, 1989]. Being a function of the relative extent of the idealized subranges (2.2),(2.3) and (2.6), the apparent "co-dimension" μ is determined by the wave age. Theoretical dependencies for the effective μ and β as functions of ξ are presented in section 4.

The low-wavenumber cutoff (the "outer scale" of the spectrum) is steep and it can be approximated by a smeared unit step function $H(k/k_0-1)$. A commonly accepted form of H(.) is given by $\exp[-(k/k_0)^{-2}]$ - as follows from the empirical Pierson-Moskowitz [1964] (P-M) spectrum. Thus, the energy-containing range is approximated by:

$$F(k) = \beta(U^2/g)^{2\mu}\, k^{-4+2\mu} \exp[-(k/k_0)^{-2}] \tag{2.7}$$

Using the dispersion relation for gravity waves, the low-frequency cut-off is related to the wave age (2.1) by:

$$k_0 = (g/U^2)\xi^{-2} \tag{2.8}$$

Typical values of ξ for open ocean waves lie in the range 2 to 3 [Glazman and Pilorz, 1990]. The limiting wave age for the "fully developed" sea still remains unknown, and the existence of the FDS state hypothesized by Kitaigorodskii [1962,1970] has been questioned both on theoretical and experimental grounds [Glazman, 1991b] along with the empirical P-M spectrum which claims to represent FDS [Pierson, 1991].

Analyzing the spatial evolution of stationary wave fields, we shall employ in sections 5 and 6 the well known empirical relationships between the wave age, ξ, the non-dimensional wind fetch, $\tilde{x}$ ($\tilde{x}=gx/U^2$ where x is the dimensional fetch), and the non-dimensional wave energy, e:

$$\xi = \mathcal{A} e^{a} \tag{2.9}$$

$$e = \mathcal{B} \tilde{x}^{b}, \tag{2.10}$$

$$\xi = C \tilde{x}^{c} \tag{2.11}$$

Sometimes these are called fetch laws. Of particular interest are variations in the values of $\mathcal{A},\mathcal{B},C,a,b$, and c revealed by comparing reports of different experimentalists. The

dimensionless wave energy (called alternatively the generalized non-dimensional fetch [Glazman, 1991b]) is defined as

$$e = \frac{\int F(\mathbf{k})d\mathbf{k}}{(U^2/g)^2} \equiv \frac{\int S(\omega)d\omega}{(U^2/g)^2} \tag{2.12}$$

Since only two of the three equations (2.9)-(2.11) are independent, we shall consider only (2.9) and (2.11). Experimental data on the parameters of the fetch laws are summarized in Table 1. Conditions characterizing individual experimental setups are highly diverse. As explained in section 5, the differences in atmospheric boundary layer stratification, in the range of the wind speed and fetch values covered, and in other factors including local depth and hydrography have effects on the parameters reported in Table 1.

Fetch laws (2.9)-(2.11) also follow from the action and energy transfer equations [Zakharov and Zaslavskii, 1983; Glazman and Srokosz, 1991]. The derivation involves certain simplifying assumptions regarding the wind input in a *developed sea* state. By a *developed sea* we understand a wave field having a broad wavenumber spectrum, such that a short-range asymptotic of the structure function $D(\mathbf{r}) \equiv \langle[\zeta(\mathbf{x}+\mathbf{r})-\zeta(\mathbf{x})]^2\rangle$ for the surface elevation field $\zeta(\mathbf{x})$ due to gravity waves reduces to [Glazman and Weichman, 1989]

$$D(r,\Theta) \approx L^{2\mu}(\mu,\Theta)\, r^{2-2\mu} \quad , \tag{2.13}$$

where the dimensional coefficient L (called the "topothesy") is independent of the spectral peak wavenumber, k_0: $L^{2\mu} = \beta(U^2/g)^{2\mu}f(\mu,\Theta)$. Since $D(r,\Theta)$ is evaluated for small spatial lags r, equation (2.13) pertains to the high-wavenumber range of the gravity wave spectrum dominated by the direct energy cascade. In particular, one can use $\mu=1/4$ and express β in terms of the Kolmogorov constant α_q. In general, (2.13) is valid if

$$(k_0 r/2)^{2\mu} \ll \mu\Gamma(\mu)/(1-\mu)^2\Gamma(1-\mu) \tag{2.14}$$

[Glazman and Weichman, 1989]. Under this condition, the field $\zeta(\mathbf{x})$ exhibits "fractal geometry" characterized by a pattern of continuously "nested" wavelets of a monotonically decreasing size. The wave slope variance, estimated as $\gamma^2 \approx D(\lambda)/\lambda^2$ where λ is the relevant (short) spatial scale of interest, becomes independent of the dominant wavelength $2\pi/k_0$. As a result, neither wind fetch nor wave age can appreciably influence γ^2. Due to the exclusive role of the wave slope for the induced air pressure and

shear stress fields (Chapter 4.2 in [Phillips, 1977]), we anticipate the wind-wave coupling to be independent of the wind fetch. Hence, in a developed sea, the mean wind U becomes the only external parameter of the wind input, and at scales satisfying (2.14) we assume a universal regime of air-sea interactions.

The wind input may be envisioned as occurring in the fashion of the Miles mechanism, i.e., being proportional to $F(\mathbf{k})$ and attaining its spectral maximum at wavenumbers above g/U^2. The integral fluxes of wave action and energy take the form:

$$P_u = \int p^+(\mathbf{k})\, d\mathbf{k} = \varepsilon R_p\, g^{-2} U^4 , \tag{2.15}$$

$$Q_u = \int q^+(\mathbf{k})\, d\mathbf{k} = \varepsilon R_q\, U^3 , \tag{2.16}$$

where $p^+(\mathbf{k})$ is the spectral density of the action input flux (per unit surface area and per unit mass of water), $q^+(\mathbf{k})$ is the spectral density of the energy flux. Both are confined to the high-wavenumber range. In the wave modeling literature, these are called the wind source functions. ε is the ratio of air and water densities. For a developed sea, the bulk transfer coefficients, R_p and R_q, are assumed to be independent of the wind fetch. If, however, one considers a broad range of sea development stages - as covered in Table 1- the assumption of constant R_p and R_q has to be relaxed to allow for a (relatively weak) dependence of these "constants" on the non-dimensional fetch. Accounting for wind-wave interaction at lower frequencies (e.g., for the feedback flux of momentum from fast-moving long waves to the atmosphere) would also result in a dependence of R_p and R_q on additional parameters.

3. Buoy observations of developed seas at equilibrium with a steady wind

The present empirical knowledge on the wave field evolution is based largely on observations at limited wind fetches and relatively small depths - as encountered in the Great Lakes, North Sea and other closed or semi-closed basins convenient for field experiments (e.g., [Toba, 1973], [Donelan et al., 1985], [Dobson et al., 1989]). These observations consistently show $\mu \approx 1/4$ and support the FDS concept with the limiting wave age, ξ_{FDS}, about 1.2. Actually, some of these observations show much greater values of the wave age [Ewing and Laing, 1987], although such cases are routinely discarded by the investigators as allegedly irrelevant to wind-driven waves. Observations in open ocean regions with stable winds and large wind fetches are relatively rare and

they report $\xi >> \xi_{FDS}$ [Glazman and Pilorz, 1990; Glazman, 1991a] and a different power law $S(\omega) \sim \omega^{-p}$, where p can reach 3 [Grose, et al., 1972].

We examined a two-year series of wind and wave observations by autonomous NOAA buoys operated by the National Data Buoy Center (NDBC). Most of the observations selected for our data set are from the Pacific trade winds zone near the Hawaiian Islands, Fig. 2. This region is characterized by large values of wind fetch and duration. A number of observations were added also from NDBC buoys in the North Atlantic - to cover cases of moderate sea states with ξ near 1.

Only the buoys of the Nomad type were used. These buoys' hulls are boat shaped, 6 m long and 3 m wide. The anemometer height is 5 m. Assuming neutral stratification of the marine boundary layer we referenced the mean wind to a standard height of 10 m. (Accounting for actual stratification would yield only an insignificant correction to the mean wind U.) The mean wind represents a 20-min average. The size of the buoys as well as the accuracy of spectral estimates allowed us to analyze the range of wave frequencies f_i from 0.03 Hz to 0.35 Hz with the Δf step of 0.01 Hz. Since these buoys provide only the frequency spectra, the directional properties of the wave field remained beyond the scope of the present work. The buoys report data on the hourly basis, with a few exceptions - when the interval is three hours.

Our consideration was limited to steady wave fields at equilibrium with the observed statistically stationary wind. The data set was prepared by browsing through thousands of continuous wave and wind observations with the goal was to discard cases in which the dominance of a given wind as the main factor determining the observed spectrum could be questioned. With practically no limitations on the length of the (hourly) records we were able to check time histories for wind speed and direction, wave spectra and wave age, as illustrated in Figs. 3-5. The cases with noticeable linear trends and, generally, all cases with relative variations of wind speed in excess of ten percent of the mean values (calculated for each six hour interval) were eliminated. The wind direction was required to remain within plus or minus 15 degree of the mean direction. Also we eliminated cases in which wave spectra showed appreciable temporal evolution (third panel from the top in Figs. 3-5). A few typical cases in which wave spectra were classified as stationary (Figs. 3 and 4) or non-stationary (Fig. 5) are illustrated. Finally, we ensured that the wave field contained no significant swell. By the swell we understand a wave system generated in a remote location by a wind field whose speed and direction are noticeably different from the local wind. To eliminate such cases, we checked the shape of wave spectra for occurrences of multiple peaks of comparable size and other conspicuous features identifying mixed seas. This procedure proved successful in an earlier study [Glazman

and Pilorz, 1990] to which the reader is referred for details and additional illustrations. The total number of "ideal" steady state cases retained for subsequent analysis was 629.

The wave age ξ was estimated using the spectral peak frequency, f_0, and mean wind U. The effective "fractal co-dimension", μ, and the generalized Phillips constant, β, were derived from the observed spectra S(f) as follows. We integrated S(f) and $f^{-1}S(f)$ numerically from a certain $f_{min} > f_0$ to the high-frequency cutoff $f_{max} = 0.35$ Hz to obtain wave energy E and action N estimates for this "equilibrium" range. Requiring that E and N coincide with the energy and action obtained by integrating the analytical wave spectrum (2.5) yields two equations for μ and β:

$$2\beta' g^2 (U/g)^{4\mu} \int_{f_{min}}^{f_{max}} f^{-5+4\mu} df = E \ , \qquad 2\beta' g^2 (U/g)^{4\mu} \int_{f_{min}}^{f_{max}} f^{-6+4\mu} df = N \ , \tag{3.1}$$

The prime in β' distinguishes this quantity from β appearing in (2.5) and (2.7) where angular frequency ω is used. Equations (3.1) have been solved by iterations considering f_{min}/f_{max} as a small parameter. Only the cases with $f_{min}/f_{max} \leq 0.7$ were used in these calculations, and only the spectra containing at least 10 frequency points within the selected range were considered. The relationship between β' and β is

$$\beta = \beta'(2\pi)^{4(1-\mu)} \tag{3.2}$$

The integration limit f_{min} must lie sufficiently above the spectral peak frequency, f_0, in order to obtain μ representative of the "equilibrium range." Practically, we selected f_{min} to be a multiple of f_0: $f_{min} = 1.5 f_0$. It was found that in the logarithmic coordinates, the typical shape of wave spectra in the given range f_{min},f_{max} is convex, i.e. $d^2(\log S)/d(\log f)^2 < 0$. Figure 6 illustrates a few typical cases. An interpretation of this observation is offered in section 4.

A more traditional way of estimating the spectral exponent and the Phillips constant is to plot the observed spectrum in logarithmic coordinates and then fit a straight line to all the points within the selected frequency range. Unfortunately, this procedure does not guarantee correct values of E and N. Besides, the μ and β so derived are sensitive to the high-frequency range of the wave spectra which may be affected by the buoy hull characteristics. In Figure 7 we illustrate the agreement between the observed spectra and the fitted power-law forms.

In Figures 8 and 9, μ and β obtained using (3.1) and (3.2) are plotted versus wave age. The plots show that ξ can exceed 3, which is well above the limit of the "fully developed sea." Evidently, a wave age greater than 2 is a typical feature of open ocean waves. Furthermore, the plots exhibit a monotonic growth of μ as the wave age increases, - tending to about 0.5 at sufficiently large ξ. As suggested in sections 5 and 6, such large values of μ (noticed first by Grose et al. [1972]) are associated with the advection of the wave energy in a spatially inhomogeneous wave field.

The high values of ξ and μ in Figs. 8 and 9 may be not the largest possible in an open ocean. When preparing our "ideal" data set, we may have unjustifiably eliminated some legitimate cases with particularly large ξ. Indeed, our requirements on the wind history were very rigid. However, this conservative choice eliminates the well-known conceptual difficulty regarding the separation of swell from a wind driven sea.

4. The shape of the wave spectrum

The observed trends in μ and β provide important clues regarding the energy balance. To better understand the connection we shall first derive the trends theoretically - based on the results of WTT for an isotropic wave field.

As was suggested earlier [Glazman and Srokosz, 1991], one can approximate the actual spectrum F(k) characterized by a gradually decreasing value of μ by a composite spectrum, $F_C(k)$:

$$F_C(k) = \begin{cases} \beta_p (U^2/g)^{2/3}\, k^{-10/3} \exp[-(k/k_0)^2] & \text{for } 0 < k \le k_u \\ \beta_q (U^2/g)^{1/2}\, k^{-7/2} & \text{for } k_u < k < \infty \end{cases} \qquad (4.1)$$

The two branches in (4.1) correspond to two basic regimes of the energy and action flow, as mentioned in section 2. Here, $\beta_{q,p}$ are universal constants which can be expressed in terms of the Kolmogorov constants (they play only an intermediate role in this derivation). The spectral peak wavenumber k_0 is given by (2.8), and the spectral maximum in the energy flux from wind to waves is assumed to occur at

$$k_u = (g/U^2)\eta^{-2} \qquad (4.2)$$

This is η^{-2}-times higher than the Phillips resonant wavenumber g/U^2. The latter, of course, is obtained by equating the mean wind speed to a wave phase velocity. The correction factor η^{-2}, which is about 2, is inspired by the Miles theory wherein the fastest

growing modes have wavenumbers greater than g/U^2. Earlier [Glazman and Srokosz, 1991], this important factor was ignored.

The requirement that the two branches of (4.1) meet at $k=k_u$ yields a relationship between the universal constants:

$$\beta_p = \beta_q \eta^{1/3} \tag{4.3}$$

Since the actual spectral shape (2.7) with $\mu = \mu(k/k_0)$ is not known, and because the experimental data provide only the overall, effective, exponent, we shall again estimate the apparent μ for the entire range. A requirement that the composite spectrum (4.1) yield the same integrated energy and action as would follow from (2.7) with a constant μ yields two equations for μ and β:

$$B\Gamma(1-\mu)\xi^{4(1-\mu)} = \Gamma(2/3,\tau)\xi^{8/3}\eta^{1/3} + (4/3)\eta^3 \tag{4.4}$$

$$B\Gamma(5/4-\mu)\xi^{5(1-\mu)} = \Gamma(11/12,\tau)\xi^{11/3}\eta^{1/3} + \eta^4 \tag{4.5}$$

where

$$B = \beta(\xi)/\beta_q \qquad \text{and} \qquad \tau = (\eta/\xi)^2 \tag{4.6}$$

Here $\Gamma(a,b)$ is the incomplete Gamma function. In the derivation of (4.5) we used the dispersion relation $\omega=\sqrt{kg}$ to eliminate ω from the spectral density of the wave action, $N(k)=F(k)/\omega$. The system (4.4),(4.5) has a simple solution, B and μ, derived in Appendix A.

Functions $B(\xi)$ and $\mu(\xi)$ are plotted in Fig. 10 for several values of η. In Fig. 11 we plot the result for $\tau=0.7$ which best agrees with the trends observed in Figs. 8 and 9. Apparently, at ξ near 1, $B(\xi)$ can be approximated (through a least-square fit) by a power law

$$B(\xi) \approx \mathcal{S}\xi^{-s} \quad , \tag{4.7}$$

which allows one to compare the theoretical prediction with the empirical data of Donelan et al. [1985]. As seen from Fig. 11, the agreement is quite good. Finally, we should emphasize that the wave-age-dependent β and μ should be viewed as *ad hoc* parameters - a consequence of a decrease in the actual value of $\mu(k/k_0)$ with an increasing distance from the spectral peak.

Apparently, within the appropriate range of the wave age values, the predicted trends are in reasonable agreement with the observations in Figures 8 and 9, while at too small

and too large ξ these WTT-based predictions disagree with the observations. At low ξ, the value of μ approaching zero can be explained by incorporating the Phillips range (2.6) into the composite spectrum model. A dynamical model describing transition from the weak turbulence regime of tetrad interactions to a regime of stronger nonlinear wave-wave interactions is offered in [Glazman, 1992]. The large values of μ approaching 1/2 at $\xi \gg 1$ are interpreted in the next two sections, along with their implications for air-sea interactions.

5. Spatially inhomogeneous wave field

Conservation of the wave action flux in the inverse cascade is consistent with the traditional understanding of the local wind-wave equilibrium as attained due to the energy dissipation at high-wavenumbers. Indeed, according to the Zakharov-Zaslavskii model [1982, 1983] (herein referred to as Z-Z), the inverse energy cascade is zero, hence the entire energy flux from wind goes toward high wavenumbers. In what follows we show that, for a developed sea state, such a simple and attractive picture is inconsistent with both the observed wave spectra and the observed wave field evolution: the large values of μ and the high values of $\mathcal{A}$, a and c in the fetch laws (2.9)-(2.11) reported in Table 1 point to a non-conservative spectral flux of wave action accompanied by a considerable leak of energy to the low-wavenumber range.

The Z-Z model for the spatial evolution of a wave field provided the first theoretical explanation of the power law (2.11) (from which the other two laws follow). The spatial evolution of a statistically stationary wave field is due to an intrinsic anisotropy of wave spectra. It is well known that the two-dimensional wave spectra $F(\mathbf{k})$ are characterized by a rather narrow angular distribution with the dominant wave propagation in the direction of the mean wind. Explanations of narrow angular spectra have been suggested by Tsimring [1989] and Zakharov and Shrira [1990]. Apparently, a preferential direction of wave propagation should result in an advective flow of the wave energy and action. The transfer of the wave action spectral density, $N=F(\mathbf{k})/\omega$, is described by

$$\nabla\cdot(\mathbf{c}_g N) + \nabla_k\cdot T(\mathbf{k}) = p \qquad (5.1)$$

where $\mathbf{c}_g = \partial\omega/\partial\mathbf{k}$ and $\nabla_k\cdot T(\mathbf{k})$ is the interaction (collision) integral for gravity waves, p is the source function for the spectral density of the wind input. Z-Z assumed that the advective term in the left-hand side has no appreciable effect on the shape of the wave spectrum, except for the value of k_0 . In other words, at $k>k_0$ the wave action flux is conserved: $\int\nabla_k\cdot T(\mathbf{k})\, d\mathbf{k}=0$ and equation (2.3) remains approximately valid for most of

the wavenumber range. Then, integrating (5.1) over all wavenumbers yields a crude model for the wave field spatial evolution

$$\nabla \cdot \int \mathbf{c}_g N d\mathbf{k} = P_u \tag{5.2}$$

where $P_u \equiv \int p \, d\mathbf{k}$ is the total input flux which is cascaded toward low wavenumbers. Assuming no variations normal to the wind vector, the spatial evolution occurs only along the fetch x. Then, substituting (2.7) with $\mu=1/3$ into (5.2) yields an equation for the spectral peak wavenumber:

$$\frac{\partial}{\partial x}\left(\frac{\alpha_p P_u^{1/3}}{2} \int_0^\infty k^{-10/3} \exp[-(k_0/k)^2] dk \right) = P_u \tag{5.3}$$

For a developed sea state, in which (2.14) holds, P_u depends only on the mean wind:

$$P_u = \varepsilon R_p g^{-2} U^4 , \tag{5.4}$$

where ε is the ratio of the air and water densities and R_p is the (constant) bulk coefficient of action transfer from wind to waves. Equation (5.4) can be obtained not only on dimensional grounds but also from a spectral model of wind input as presented in Appendix B. The non-dimensional wind fetch is defined as

$$\tilde{x} = gx/U^2 \tag{5.5}$$

Using (2.8) and (5.4), an exact solution of (5.3) takes the form of equation (2.11) with

$$c = 3/14, \qquad C = [4(\varepsilon R_p)^{2/3}/\alpha_p \Gamma(7/6)\,]^{3/14} \tag{5.6}$$

[Zakharov and Zaslavskii, 1983]. Expressions (2.9) and (2.10) for the non-dimensional wave energy e are derived by substituting (2.7) with $\mu=1/3$ into the integral (2.12) and using (2.11) and (5.6). Thus we arrive at

$$a = 3/8 , \qquad \mathcal{A} = [\alpha_p (\varepsilon R_p)^{1/3} \Gamma(2/3)/2]^{-a} \tag{5.7}$$

Comparing the exponents a, c with the data in Table 1 we find appreciable discrepancy with all experiments. Partly this might be due to the fact that many of the observations in Table 1 are dominated by cases of moderately developed seas with $\xi \leq 1$. For such cases, the direct energy cascade dominates wave dynamics, and the assumption $\int \nabla_k \cdot T(\mathbf{k})\, d\mathbf{k}=0$ must be replaced with the corresponding statement for the spectral energy flux: $\int \nabla_k \cdot T(\mathbf{k})\, \omega d\mathbf{k}=0$. However, a more interesting, additional, source of the discrepancy, as suggested in the following sections, is due to the fact that the Kolmogorov spectra (2.2) ignore the advective transfer of the wave action. Hence, they would not be valid even if the inverse cascade did dominate the wave dynamics.

In the absence of ambient currents and sea level variations, the integrated energy balance, provided the spectral energy flux in the direct cascade is (approximately) conserved, can be approximated by [Glazman and Srokosz, 1991]:

$$\nabla \cdot \int \mathbf{c}_g F(\mathbf{k},x) d\mathbf{k} = \Delta Q \tag{5.8}$$

where $\Delta Q \equiv \int (q^+ + q^-) d\mathbf{k}$ is the net integrated input of the wave energy (wind input minus small-scale dissipation). Assuming ΔQ to be proportional to U^3 one arrives ultimately at :

$$\frac{\partial}{\partial x} \frac{\beta}{2} g^{3/2} (U^2/g)^{2\mu} \int_0^\infty k^{-7/2+2\mu} \exp[-(k_0/k)^2] dk = \varepsilon R_q U^3 \tag{5.9}$$

where the general form (2.7) was used for the wave spectrum, and R_q is the bulk coefficient of the net energy input. For the wind input, the form $\varepsilon R_q^+ U^3$ is confirmed by empirical source functions - as shown in Appendix B, while the breaking wave dissipation term $\int q^-(\mathbf{k}) d\mathbf{k} \propto U^3$ is justified, for instance, by Phillips [1985]. In this formulation the integral energy balance is controlled by both the advective transfer due to the wave group velocity and the growth of the dominant wavelength with fetch due to nonlinear wave-wave interactions.

Integrating (5.9) over relatively short segments of x, over which R_q can be assumed constant [Glazman and Srokosz, 1991], one finds the solution in the form (2.11) with

$$c = 1/(5-4\mu) \ , \qquad C=[4\varepsilon R_q/\beta\Gamma(5/4-\mu)]^c \tag{5.10}$$

Using (2.7), equations (2.9) and (2.12) yield:

$$a = 1/(4-4\mu)\,, \qquad \mathcal{A} = [\beta\Gamma(1-\mu)/2]^{-a} \tag{5.11}$$

For $\mu = 1/4$ this is:

$$a = 1/3\,, \qquad \mathcal{A} = (0.613\beta)^{-1/3}\,, \tag{5.12}$$

and equations (5.10) become:

$$c = 1/4\,, \qquad C = [4\varepsilon R_q/\beta]^{1/4} \tag{5.13}$$

Evidently, these values are closer to the data of Table 1 than are the values given by (5.6) and (5.7).

Variations of the coefficients in Table 1 can be explained based on (5.10) and (5.11) - as a result of variations in the effective value of μ. In Figures 12 and 13, the data of Table 1 are plotted as points on the planes $\{c,C\}$ and $\{a,\mathcal{A}\}$. To compare these with the predicted trends, we also plot functions $C=f_1(c)$ and $\mathcal{A}=f_2(a)$ derived from (5.10) and (5.11) by eliminating μ. Parameters β and R_q which provide the best fit to the experimental points are: $\beta \approx 3\ 10^{-3}$ and $R_q \approx 4.\ 10^{-5}$. While this value of β is in agreement with the data, the coefficient R_q is not known from direct measurements. In Appendix B this coefficient is shown to be consistent with empirical data on the wind input spectral flux $q^+(\omega)$. The varying μ required for the explanation of the observed trends is associated with a (relatively weak) dependence of μ on ξ - as predicted in section 4. Hence, the trends found in Table 1 are explained by the fact that different experiments covered different (although overlapping) ranges of the wave age. This was so not only because of different wind fetch and wind speed ranges covered by different observations but also because of differences in atmospheric boundary layer stratification (in different regions and seasons) which affects the values of R_q and R_p. Indeed, coefficients R_q and R_p can be included into the fetch to highlight their role as a scaling factor in equations (5.3) and (5.9).

In conclusion, let us show that the main results (5.10) and (5.11) can be further refined by adding a feature consistent with our previous observations. Specifically, let us account for possible effect of a wave-age-dependent β on the fetch laws' coefficients. Such a correction becomes particularly relevant for moderate sea states with ξ near 1. To this end we notice that, while allowing β to be a function of the wave age - hence of the wind fetch x - in the left-hand side of (5.12), we may not have to worry about a corresponding refinement of the wind-wave interaction coefficient in the right-hand side. As suggested in the end of section 2, the wind input can be approximately treated as

being independent of the fetch. According to both the observed and the predicted trends, Figures 9 and 11, the range of ξ in which β experiences most of its variation ends at about $\xi \approx 1.5$. In this regime of moderately developed seas, β can be approximated by a power law (4.7) where $s \approx 0.5$ and $\mathcal{S} \approx 1$. Then, equation (5.9) yields:

$$c = 1/(5-4\mu - s) \ , \qquad C=[4\varepsilon R_q/\beta_0\Gamma(5/4-\mu)]^c \ , \tag{5.14}$$

and in place of (5.11) we find:

$$a = 1/(4-4\mu - s) \ , \qquad \mathcal{A} = [\beta_0\Gamma(1-\mu)/2]^{-a} \tag{5.15}$$

Evidently, the refinement is in the right direction, although it does not alter the result in a crucial way.

6. Effect of energy and action advection on the spectral shape

Evidently, the simple theory presented above explains many features of the wave field spatial evolution. However, the assumption that the term $\nabla\cdot(\mathbf{c}_g E)$ in the energy transfer equation (or term $\nabla\cdot(\mathbf{c}_g N)$ in (5.1)) has no influence on μ is not always justified. Indeed, the values of μ yielding best agreement with the data are generally greater than those obtained with Kolmogorov-type spectra. In Figure 14 we plot c and C, given by (5.10), versus μ - to show that the range of μ implicit in Figures 12 and 13 overlaps but does not coincide with that based on the purely inertial spectra (2.2) and (2.3). This is also evident from our direct observations, Fig. 8. Greater values of μ called for by these comparisons can be explained as follows.

The group velocity term in (5.1) (and a similar term in the spectral energy balance) describes a loss of wave action (energy) from a given spectral band due to the advective transport. The effect is stronger at lower frequencies for which $\mathbf{c}_g$ is greater. Therefore, the lower-frequency spectral components loose wave action (energy) at a faster rate than do the higher-frequency components. This should lead to a flattening of the spectral density function, hence to an increase of the apparent μ. Let us assess effectiveness of this mechanism.

The characteristic time t_c associated with the action (or energy) advective transfer is found by scaling the advective term in the transfer equation (5.1). This yields

$$t_c^{-1} \sim \frac{\omega}{2kx*} \tag{6.1}$$

where $x*$ is the characteristic spatial scale of the problem, which of course is the wind fetch. The characteristic time for the action (or energy) spectral transfer due to nonlinear wave-wave interactions in the resonant wave tetrads is given by (e.g., [Kitaigorodskii, 1983]):

$$t_n^{-1} \sim \omega(ak)^4 \tag{6.2}$$

where ak is the steepness of the wavelets on scale k. The ratio

$$\frac{t_c}{t_n} \sim 2(ak)^4 \, kx* \tag{6.3}$$

provides a measure of the relative importance of the non-linear four-wave resonant interactions as compared to the advective transfer. At high wavenumbers, the wave steepness is higher than that at low wavenumbers, - due to the statistical self-affinity of the wave profiles [Glazman and Weichman, 1989]. Hence, at a large wind fetch, the collision integral dominates dynamics of short gravity waves. However, at wavenumbers of order g/U^2 , i.e. below the generation range, (6.3) is estimated as $2\gamma^4 \, \text{ɤ}$, and the characteristic wave slope variance γ^2 is of order 10^{-3} . Therefore, at non-dimensional fetch $\text{ɤ} < 10^5$, effects of the wave field spatial inhomogeneity resulting in the advective transfer of wave energy and action must be taken into account. These effects are expected to raise the effective value of μ above 1/3 by removing energy from the low-wavenumber range at a greater rate than from higher wavenumbers.

7. Conclusions

Even in its present "naive" form, WTT explains, at least qualitatively, many phenomena in wind-generated gravity waves observed in open ocean. However, a number of important issues remain unclear. These include the limiting shape of the wave spectrum as the fetch tends to infinity and, more generally, the relevance of the FDS concept for ocean waves. Also, additional effort is required to understand the role of the angular spectrum and the effect of wave field's anisotropy on the energy and momentum exchange between the wind field and the fields of surface gravity waves and underlying larger-scale motions.

Anisotropy of the wave field plays a special role. By providing the necessary condition for an advective transfer of energy in the direction of the dominant wave propagation it modifies the energy balance. In place of a purely inertial inverse cascade of the wave action with a zero spectral flux of energy (as follows from WTT for an

isotropic steady-state wave field), a non-conservative energy flux to the low wavenumber range becomes possible. Ultimately, the energy is advected away from the wave generation region. One consequence is that the local dissipation by breaking waves and molecular viscosity acting at high frequencies is not the only, and possibly not even a major, mechanism of energy loss. Indeed, the bulk coefficient R_q for the net energy input (wind input minus high-frequency dissipation) - estimated indirectly in section 5 - does not appear to be noticeably smaller than the coefficient R_q^+ for the wind input alone - estimated in Appendix B. Other, essentially non-local, mechanisms (e.g., wave interactions with Langmuir circulation, internal waves, meso-scale eddies, ocean currents, etc.) may be equally or even more important for the energy extraction from the wave field. Accounting for such mechanisms requires inclusion of terms like $\rho g(d+h)\nabla h$ into the momentum transfer equation, where h is an averaged (over the dominant wave cycle) surface height and d may be the depth of the upper mixed layer or of the thermocline. In the energy transfer equation the terms like $\nabla(\mathbf{FU})$ and $\mathbf{S}(\mathbf{k}):\nabla\mathbf{U}$, where $\mathbf{S}(\mathbf{k})$ is the spectral density of the excess momentum flux tensor (including the radiation stress tensor), are required (Chapter 3.6 of [Phillips, 1977]). Depending on the nature of "large-scale" fields h and **U**, various coupled problems can be studied to identify effective mechanisms of wind-wave equilibrium. The ability of a wave field to induce larger-scale motions may have important implications for ocean-atmosphere coupling.

ACKNOWLEDGMENTS. This work was performed at the Jet Propulsion Laboratory, California Institute of Technology, under contract with the National Aeronautics and Space Administration. Financial support was provided by the Office of Naval Research. The author thanks Alexander Greysukh of JPL for carrying out the data compilation and extensive calculations resulting in Figures 2-9.

APPENDIX A: Solution of (4.4) and (4.5).

Divide (4.5) by (4.4), multiply the result by ξ, and denote the right-hand side of the resultant equation by $\Psi(\xi,\eta)$:

$$\Gamma(5/4-\mu)/\Gamma(1-\mu) = \Psi(\xi,\eta) \qquad (A.1)$$

The left-hand side can be simplified by expanding it in Taylor series about $\mu = 0$ and neglecting terms higher than μ^2. Alternatively, one can fit a quadratic polynomial to this function to find:

$$\Gamma(5/4-\mu)/\Gamma(1-\mu) \approx 0.9058 - 0.3022\mu - 0.2295\mu^2 \qquad (A.2)$$

Then, the solution of (4.4) and (4.5) is found in a closed form as:

$$\mu \approx -0.6584+(4.3801-\Psi(\xi,\eta)/0.22951)^{1/2} \qquad (A.3)$$

Once μ has been found, obtaining $B(\xi)$ is a trivial task.

APPENDIX B: Empirical Data On R_q^+

Experimentalists usually measure the spectral density, q^+, of the energy flux from wind to waves, and denote it by S_{in}. Unfortunately, such measurements - conducted in coastal regions - are available only for poorly developed sea states (wave age well under 1). Let us employ first an empirical form of $S_{in}(\omega)$ due to Snyder et al. [1981], and compare its integrated value to the net integrated energy flux, Q, in (5.9). Thus we use

$$S_{in} = \max[0, C_q\varepsilon(U\omega/g-1)\omega g F(\mathbf{k})] \qquad (B.1)$$

where C_q=0.25±0.7. Replacing ω with $(kg)^{1/2}$ and using (2.7), the integration over all wavenumbers yields

$$Q_{in} = \int S_{in}\, d\mathbf{k} = \varepsilon R_q^+ U^3 \qquad (B.2)$$

where the bulk coefficient of the (pure) wind input is

$$R_q^+ = \beta C_q[(1-2\mu)(3-4\mu)]^{-1} \qquad (B.3)$$

At the low degree of wave development characterizing Snyder's et al. observations, the appropriate value of μ is near zero and $\beta \approx 10^{-2}$. Therefore, $R_q^+ \sim 10^{-3}$ which is much greater than the value of R_q predicted in section 5. Apparently, under such conditions, the high-frequency-dissipation component of R_q is very important. The Snyder et al. observations were conducted in the Bay of Abaco with the local depth of 9 m and wind

fetch within 10 km. Under such conditions, the waves are generally steeper than those in a developed sea, which explains why these observations show large input flux.

In the observations by Hsio and Shemdin in the North Sea [1983] the wave field was more mature and the corresponding empirical source function was found to be:

$$S_{in} = \max[0, C_q\varepsilon(U\omega/g-1)^2\omega g F(\mathbf{k})] \tag{B.4}$$

where the empirical coefficient C_q is 0.12. The local depth, 18 m, in this experiment was still insufficient, although the fetch was greater than in Snyder's et al. experiments. Al-Zanaidi and Hui [1984] used (B.4), however they found that the appropriate value of C_q varies between 0.04 and 0.06. It can be shown also that the empirical data summarized by Plant [1982] are equivalent to $C_q \approx 0.03$. Phillips [1985] demonstrated that C_q of this magnitude is consistent with certain other semi-empirical constants characterizing wind-wave interactions, whereas larger values would lead to considerable discrepancy.

Recently, an exact regime of tetrad wave-wave interaction in the direct energy cascade, given wind input (B.4), was established theoretically [Glazman, 1992]. The maximum value of C_q compatible with this regime follows from (6.12) of [Glazman, 1992]:

$$C_q = \frac{\beta^2}{\varepsilon} \tag{B.5}$$

With $\varepsilon \approx 10^{-3}$ and $\beta \approx 5.10^{-3}$ - as found from Fig. 9 at $\xi \approx 1$ - we estimate $C_q \approx 2.5\ 10^{-2}$. This small value lends further credibility to the suggestion that, for deep-water waves considered in the present work, the correct values of C_q lie in the range 0.02 to 0.04, yielding $R_q^{\dagger} \approx R_q$ of section 5. In other words, the negative (high-frequency dissipation) component of the net energy flux seems to be negligible compared to the wind input flux.

REFERENCES:

Al-Zanaidi, M.A. and Hui, W.H., 1984. Turbulent airflow over water waves - a numerical study. J. Fluid Mech., 148, 225-246.

Dobson, F., W. Perrie, and B. Toulany, 1989. On the deep-water fetch laws for wind-generated surface waves. J. Atmosphere-Ocean, 27(1), 210-235.

Donelan, M.A., J. Hamilton, and W.H. Hui, 1985. Directional spectra of wind-generated waves. Phil. Trans. R. Soc. London, A 315, 509-562.

Glazman, R.E., 1991a. Statistical problems of wind-generated gravity waves arising in microwave remote sensing of surface winds. Trans. Geosci. Rem. Sensing. 29(1), 135-142.

Glazman, R.E., 1991b. Reply. J. Geophys. Res., 96(C3), 4979-4983.

Glazman, R.E., 1992. Multiwave interaction theory for wind-generated surface gravity waves. Journ. Fluid Mech., vol. 243, 623-635.

Glazman, R.E., G.G. Pihos and J. Ip, 1988. Scatterometer wind-speed bias induced by the large-scale component of the wave field. J. Geophys. Res., 93(C2), 1317-1328.

Glazman, R.E., and S.H. Pilorz, 1990. Effects of sea maturity on satellite altimeter measurements. J. Geophys. Res., 95(C3), 2857-2870.

Glazman, R.E., and P. Weichman, 1989. Statistical geometry of a small surface patch in a developed sea. J. Geophys. Res., 94(C4), 4998-5010.

Glazman, R.E., and M.A. Srokosz, 1991. Equilibrium wave spectrum and sea state bias in satellite altimetry. Journ. Phys. Oceanogr., 21(11), 1609-1621.

Grose, P.L., K.L. Warsh and M. Garstang, 1972. Dispersion relations and wave shapes. J. Geophys. Res., 3902-3906

Hasselmann, K. On the non-linear energy transfer in a gravity-wave spectrum. J. Fluid Mech., 12, 481-500, 1962.

Hasselmann, K. et XV al., 1973. Measurements of wind wave growth and swell decay during the Joint North Sea Wave Project (JONSWAP). *Herausgegeben vom Deutsch. Hydrograph. Institut., Reihe A,* no. 12, 95 pp.

Hsiao, S.V. and O. H. Shemdin, 1983. Measurements of wind velocity and pressure with a wave follower during MARSEN. J. Geophys. Res., 88(C14), 9841-49.

Kahma, K.K., 1981. A study of the growth of the wave spectrum with fetch. J. Phys. Oceanogr., 11, 1503-1515.

Kitaigorodskii, S.A., 1962. Applications of the theory of similarity to the analysis of wind-generated wave motion as a stochastic process. Izv., Geophys. Ser. Acad. Sci., USSR, 1, 105-117

Kitaigorodskii, S.A., 1970. Fizika vzaimodestviya atmosferi i okeana (Physics of air-sea interaction). Leningrad: Gidrometeoizdat. (Engl. Transl.(1973). Jerusalem: Israel Prog. Sci. Transl.)

Kitaigorodskii, S.A., 1983. On the theory of the equilibrium range in the spectrum of wind-generated gravity waves. J. Phys. Oceanogr., 13, 816-827.

Liu, P.C. and D.B. Ross, 1980. Airborne measurements of wave growth for stable and unstable atmospheres in Lake Michigan. J. Phys. Oceanogr. 10(11), 1842-1853.

Mitsuyasu,H., R.Nakayama, and T.Komori, 1971. Observations of the wind and waves in Nakata Bay. Rep. Res. Inst. Appl. Mech., Kyushu Univ., 19,37-74.

Pierson,W.J., 1991. Comment. J. Geophys. Res., 96(C3),4973-4977.

Pierson,W.J. and L. Moskowitz, 1964. A proposed spectral model for fully developed wind seas based on the similarity theory of S.A. Kitaigorodskii. J. Geophys. Res., 69, 5181-5190.

Phillips, O.M. The Dynamics Of The Upper Ocean, 2nd edition, Cambridge Univ. Press, New York, 336 pp., 1977.

Phillips, O. M., 1985. Spectral and statistical properties of the equilibrium range in wind-generated gravity waves. J.Fluid Mech., 156, 505-531.

Ross , D.B., 1978. On the use of aircraft in the observation of one- and two-dimensional ocean wave spectra. Ocean Wave Climate, M.D.Earle and A. Malahoff, Eds., Plenum Press, 253-267.

Snyder, R.L., F.W.Obson, J.A.Elliot, and R.B.Long, 1981. Array measurements of atmospheric pressure fluctuations above surface gravity waves. J. Fluid Mech., 102,1-59.

Toba, Y., 1973. Local balance in the air-sea boundary processes, III, On the spectrum of wind waves. J. Oceanogr. Soc. Jpn, 29, 209-220.

Tsimring, L.S., 1989. Formation of a narrow angular spectrum of wind-driven waves for a nonlinear interaction between wind and waves. Izvestiya, Atmos. Ocean. Physics, 25(4), 300-306.

Walsh, E.J., D.W. Hanckock III, D.E. Hines, R.N. Swift, and J.F. Scott, 1989. An observation of the directional wave spectrum evolution from shoreline to fully developed. Journ. Phys. Oceanogr., 19(5), 670-690.

Zakharov, V.E. and N.N. Filonenko, 1966, The energy spectrum for stochastic oscillation of a fluid's surface. Doklady Academii Nauk S.S.S.R., 170(6), 1292-1295, (in Russian)

Zakharov, V.E. and M.M. Zaslavskii, 1982. The kinetic equation and Kolmogorov spectra in the weak turbulence theory of wind waves. Izvestiya, Atmospheric and Oceanic Physics (English Translation), 18(9), 747-753

Zakharov, V.E. and M.M. Zaslavskii, 1983. Dependence of wave parameters on the wind velocity, duration and its action and fetch in the weak-turbulence theory of wind waves. Izvestiya, Atmospheric and Oceanic Physics (English Translation),19(4), 300-306

Zakharov, V.E. and V.I. Shrira, 1990. On the formation of the directional spectrum of wind waves. Zhurnal Eksperimentalnoi I Teoreticheskoi Fiziki, Vol. 98(6), 1941-1958.

Table 1

Field observations

Data source	$\xi = \mathcal{A}e^{a}$		$e = \mathcal{B}\tilde{x}^{b}$		$\xi = C\tilde{x}^{c}$	
	$\mathcal{A}$	a	$\mathcal{B}\times 10^{-7}$	b	C	c
Dbsn	5.62	0.29	12.7	0.75	0.094	0.24
JONSWAP	7.94	0.33	1.6	1.0	0.045	0.33
Dnln	5.98	0.30	8.4	0.76	0.086	0.23
Phlps			1.6	1.0	0.089	0.25
Rss			1.2	1.1	0.084	0.27
Wlsh			1.9	1.0	0.069	0.29
Kahma					0.050	0.33
Mitsu			2.89	1.0	0.051	0.33
Glzmn	7.65	0.31				

Abbreviation of data sources: Dbsn: [Dobson et al., 1989], JONSWAP: [Hasselmann et al., 1973], Dnln: [Donelan et al., 1985], Phlps: [Phillips, 1977], Rss: [Ross, 1978] and [Liu and Ross, 1980], Wlsh: [Walsh et al. 1989], Kahma: [Kahma, 1981], Mitsu: [Mitsuyasu et al., 1971], Glzmn: [Glazman, 1991a].

Captions for Figures.

Figure 1. Wavenumber subranges in an equilibrium spectrum of developed seas. Thin solid straight lines represent power-law approximations, in the form $k^{-4+2\mu}$, for the specific wavenumber subranges: μ decreases with an increasing distance away from the spectral peak wavenumber k_0. The thick-dash line represents a power law approximation for the entire equilibrium range: the "effective value" of μ is determined by the relative extent of the constituent subranges.

Figure 2. Locations of main (Hawaiian) NDBC buoys used in the data set.

Figure 3. Time history of wind vector, wave spectrum and wave age observed at buoy 51003, illustrating a steady-state wave field at equilibrium with a given wind. Top panel: wind vector; second panel: wind speed in m/s; third panel: contour plot of the wave frequency spectrum evolving in time; bottom panel: wave age estimated using (2.1) where U and ω_0 are based on hourly buoy reports.

Figure 4. The same as Fig. 4, buoy 51002

Figure 5. Example of an unsteady sea state. See caption for Figure 3.

Figure 6. Typical shapes of statistically stationary wave spectra S(f) observed near the Hawaiian Islands.

Figure 7. Empirical fit to the equilibrium range of wave spectra in the form of (2.5) for which the effective values of μ and β are calculated using (3.1). Solid curves are the observed wave spectra: (1) at wind speed 11.8 m/s and wave age 1.9, (2) at wind speed 11.8 and wave age 2.2. Dashed curves: empirical fit (2.5).

Figure 8. The apparent "fractal co-dimension" μ versus wave age ξ calculated from (3.1) and (3.2) for 629 spectra.

Figure 9. The generalized Phillips constant β versus wave age ξ calculated from (3.1) and (3.2).

Figure 10. Analytical solution of (4.4),(4.5) for three values of τ. Solid curves: τ=0.9. Short-dash curves: τ=0.8. Long-dash curves: τ=0.7.

Figure 11. Solid and short-dash curves: solution of (4.4),(4.5) at τ=0.75 – for $B(\xi)$ and μ, respectively. Long-dash curve: a regression curve approximating $B(\xi)/4$ by (4.7) for a range of ξ from 0.9 to 1.2. This empirical fit, characterized by $s \approx 0.5$, agrees with the Donelan's et al. [1985] $s \approx 0.55$.

Figure 12. Parameters in equation (2.11). Solid curve: C as a function of c obtained by eliminating μ from equations (5.10). Numerical constants providing the best fit to the data points are: β=3 10^{-3}, R_q= 4 10^{-5}. Diamonds: experimental data from Table 1. The diamond marked by "W" represents the data of Walsh et al. [1989] who claim to have observed the fully developed sea state.

Figure 13. Parameters in equation (2.9). Solid curve: $\mathcal{A}$ as a function of a obtained by eliminating μ from equations (5.11); diamonds: experimental data from Table 1. See also the caption for Fig. 12.

Figure 14. Theoretical dependence of c and C on μ, eq.(5.10). Notice the range of μ .

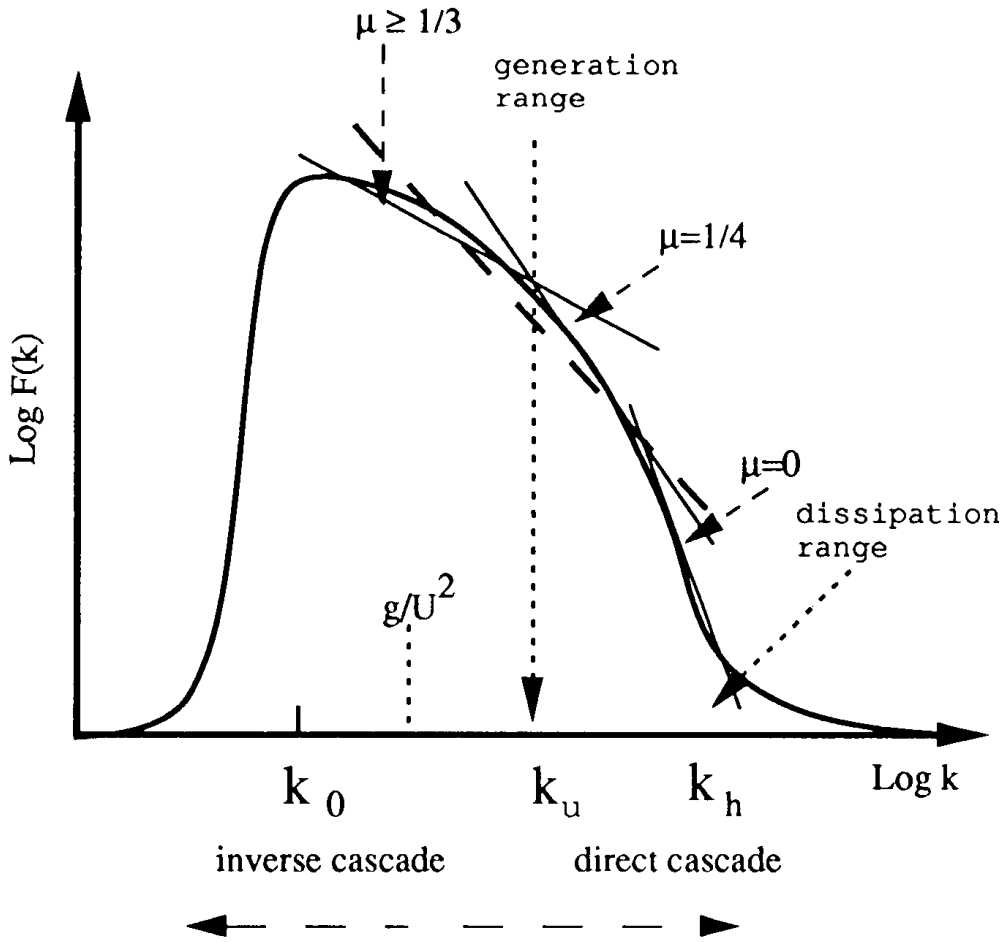
μ ≥ 1/3
generation range
μ=1/4
μ=0
dissipation range
Log F(k)
g/U2
k 0
k u
k h
Log k
inverse cascade
direct cascade

Fig. 1

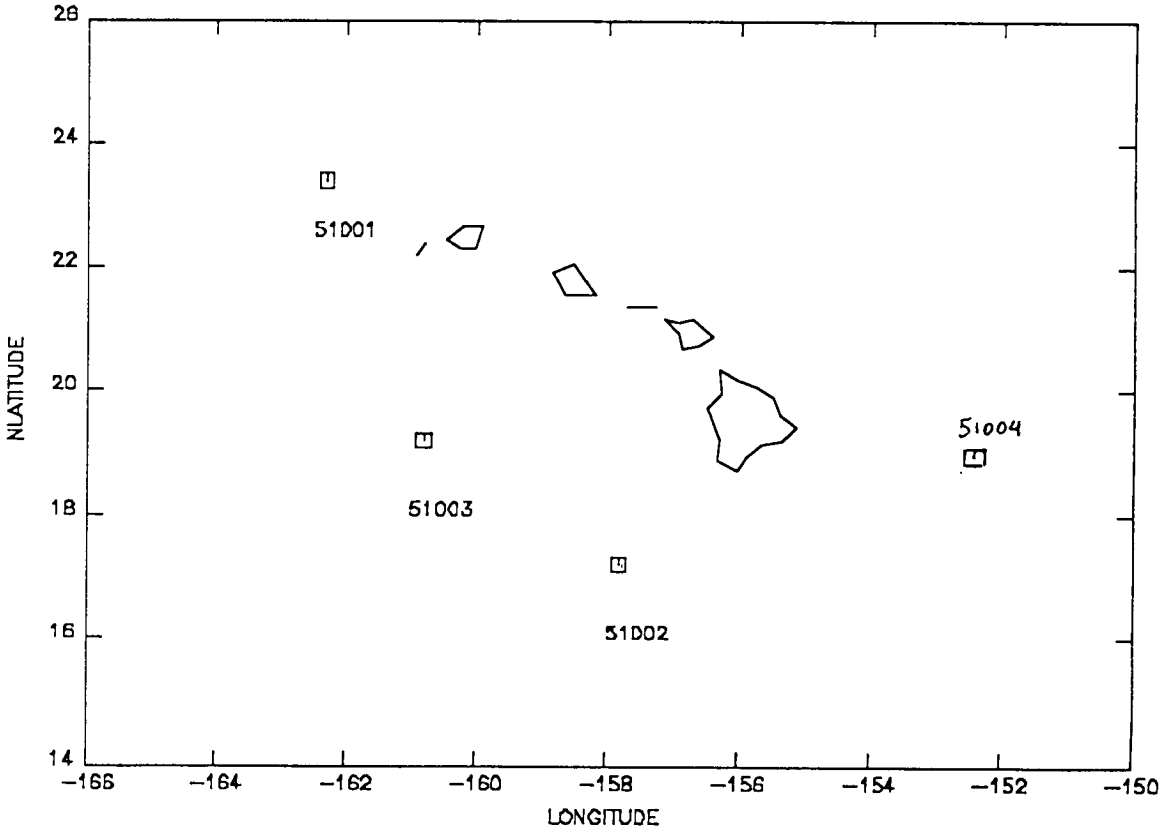
26
24
22
20
18
16
14
NLATITUDE
51001
51003
51004
51002
−166
−164
−162
−160
−158
−156
−154
−152
−150
LONGITUDE

Fig. 2

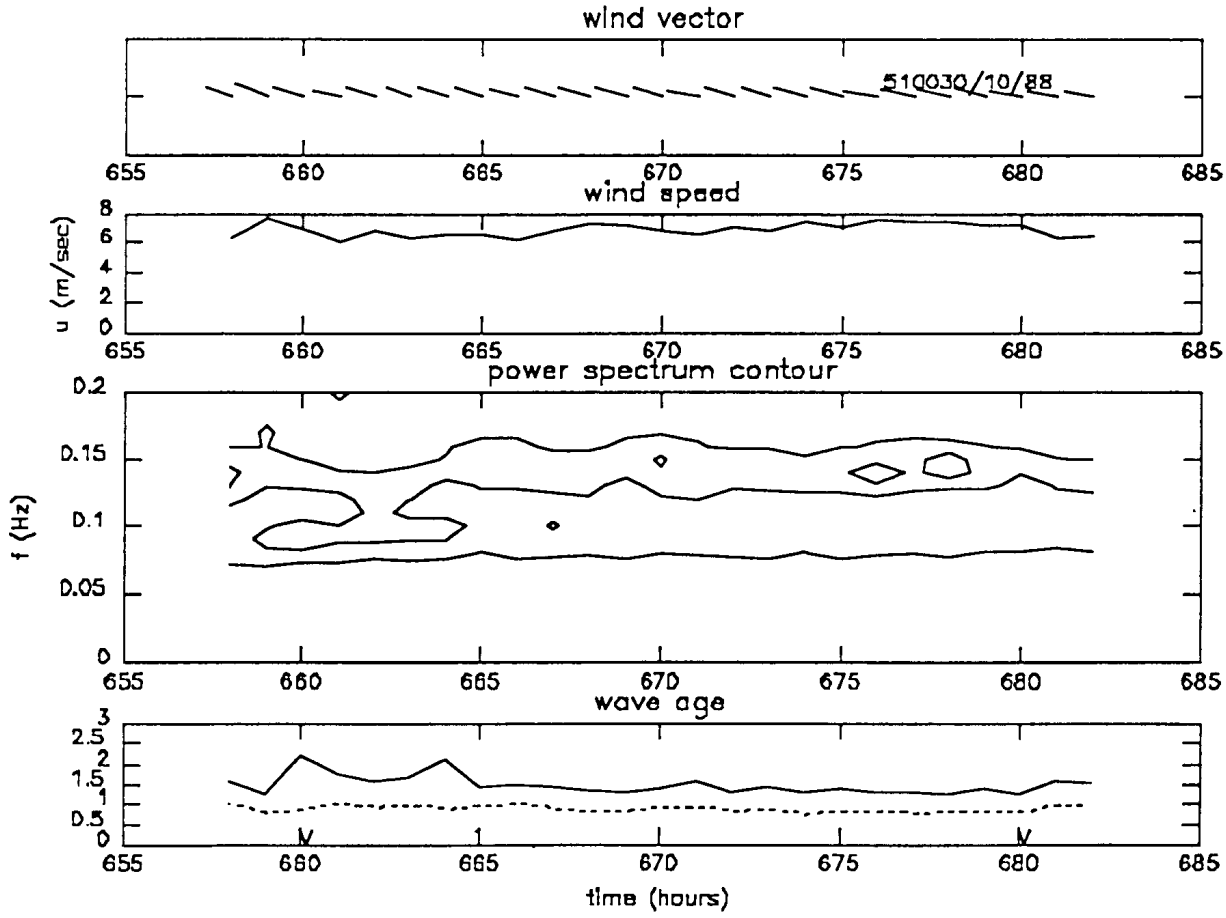
wind vector
510030/10/88
655
660
665
670
675
680
685
wind speed
u (m/sec)
8
6
4
2
0
power spectrum contour
f (Hz)
0.2
0.15
0.1
0.05
0
wave age
3
2.5
2
1.5
1
0.5
0
time (hours)

Fig. 3

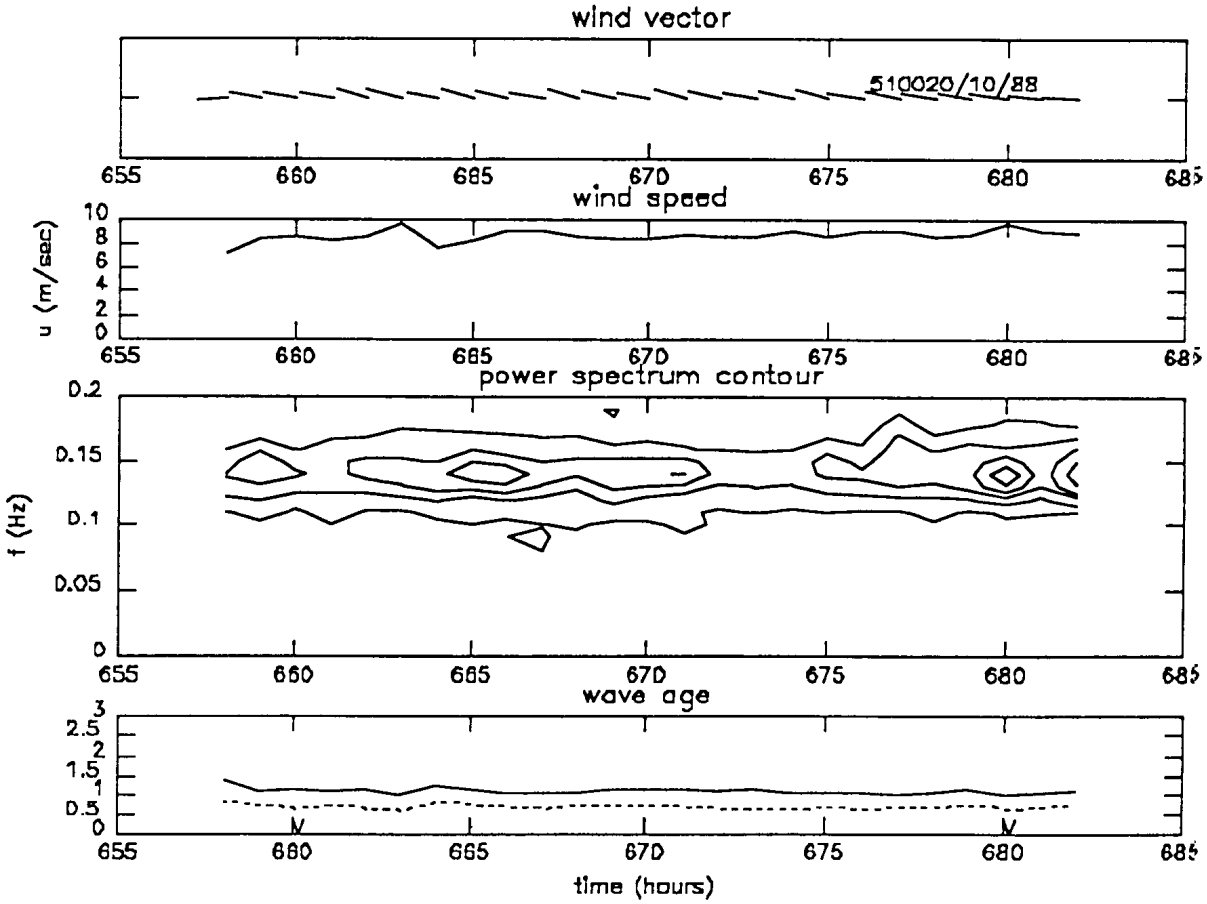
wind vector
510020/10/88
655
660
665
670
675
680
685
wind speed
u (m/sec)
10
8
6
4
2
0
power spectrum contour
f (Hz)
0.2
0.15
0.1
0.05
0
wave age
3
2.5
2
1.5
1
0.5
0
time (hours)

Fig. 4

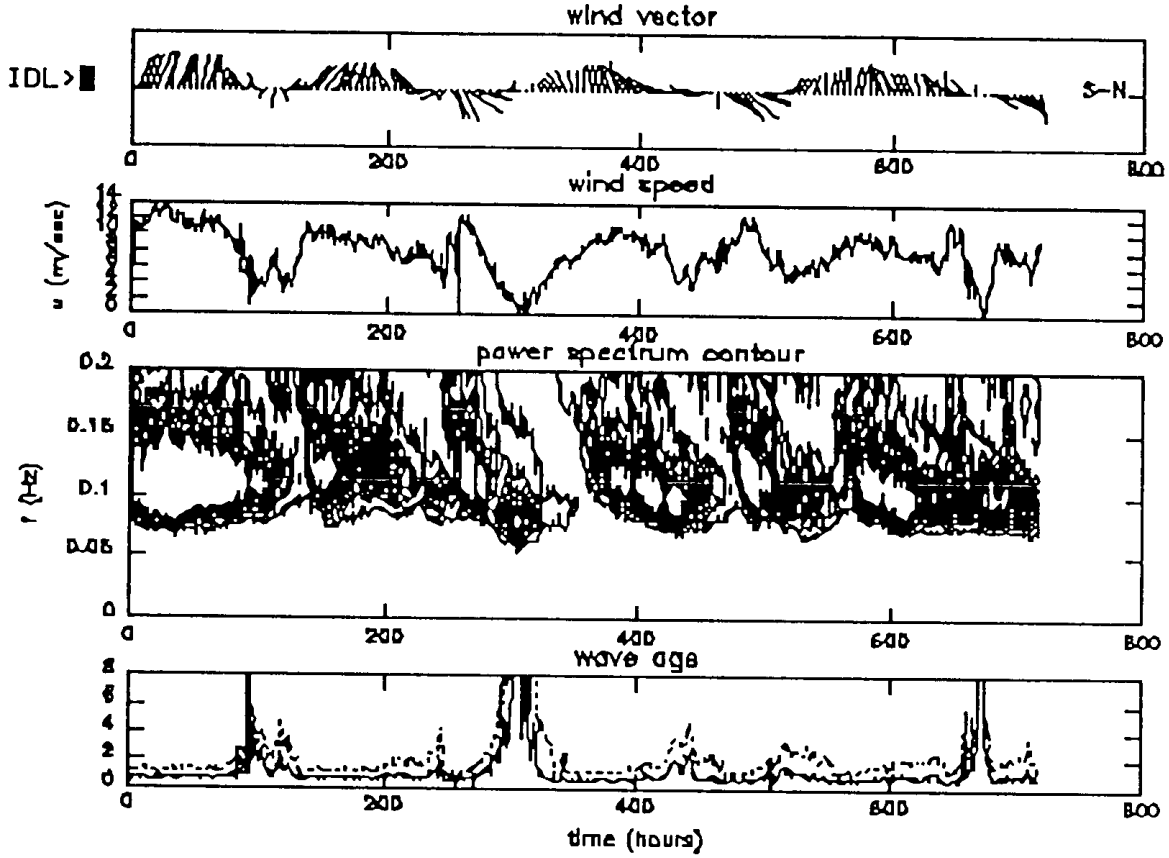
wind vector
IDL>
S-N
0
200
400
600
800
wind speed
u (m/sec)
power spectrum contour
f (Hz)
0.2
0.15
0.1
0.05
0
wave age
8
6
4
2
0
time (hours)

Fig 5

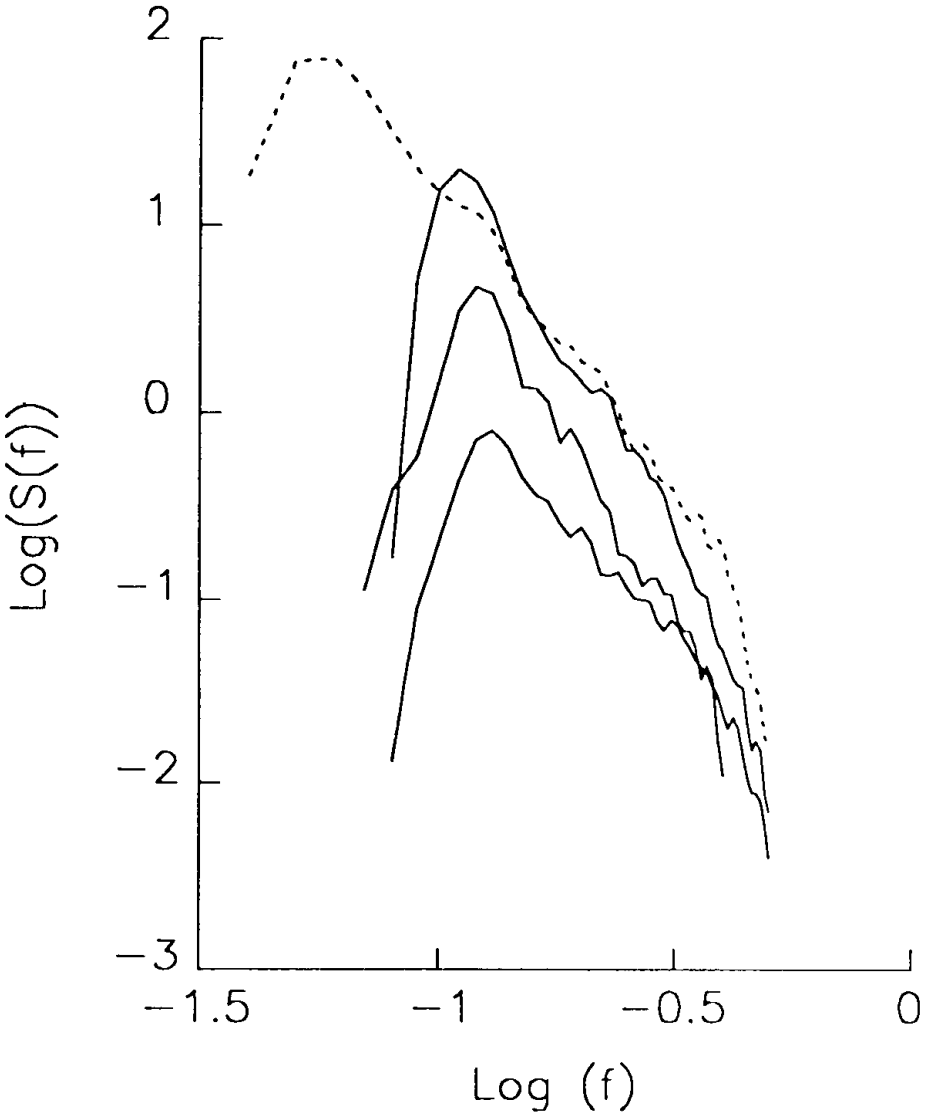

Fig. 6

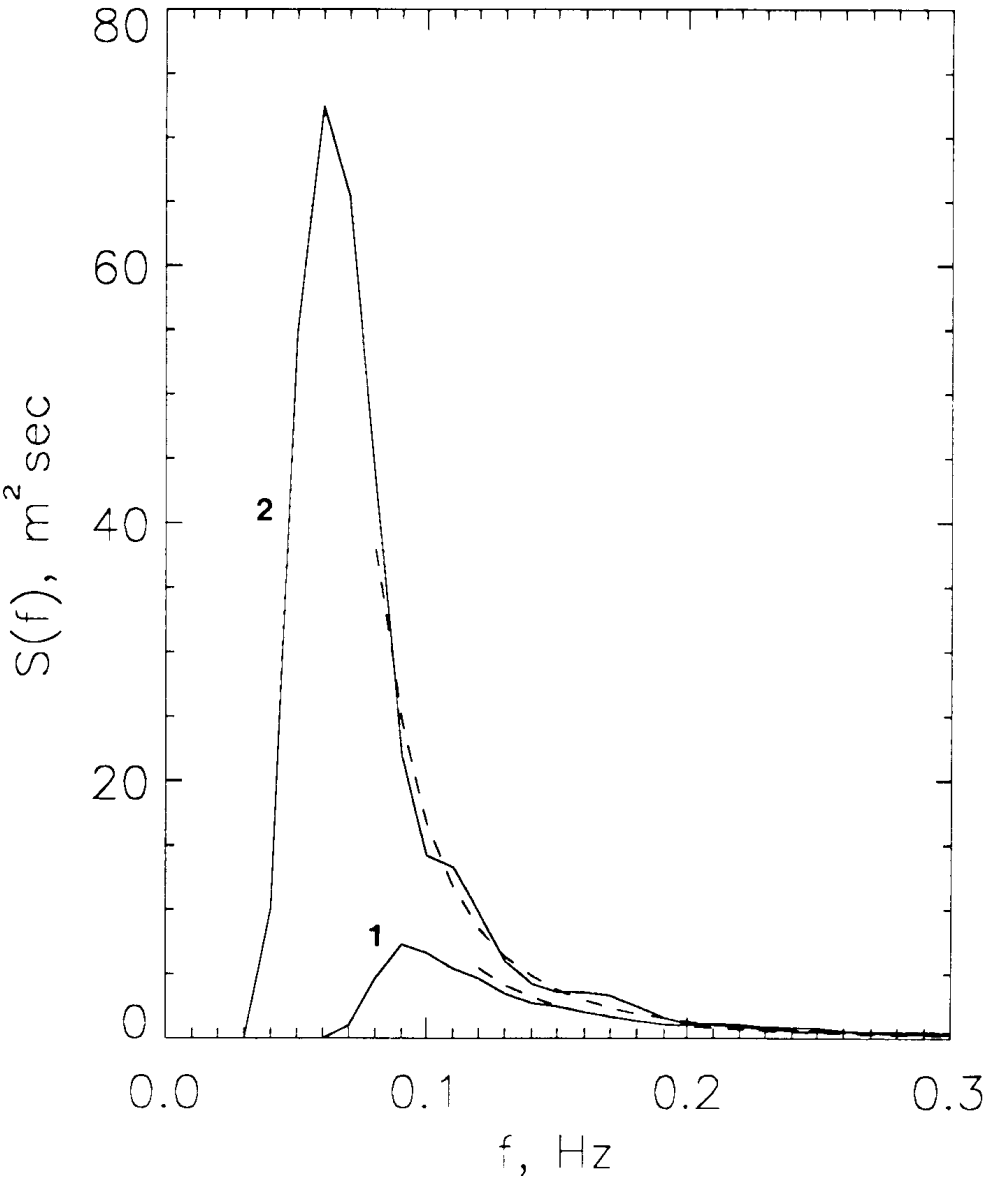
80
60
40
20
0
S(f), m² sec
2
1
0.0
0.1
0.2
0.3
f, Hz

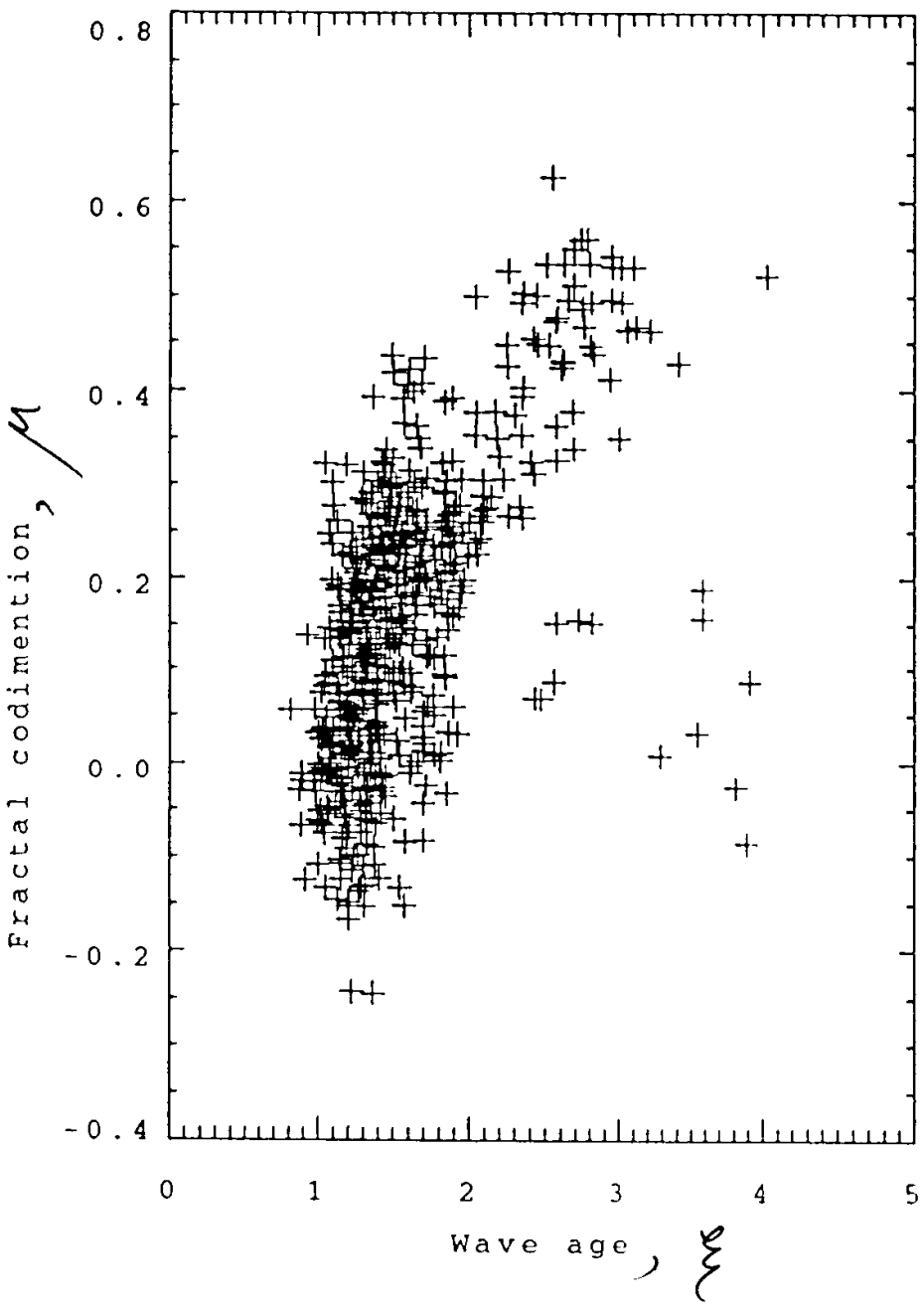

Fig. 8

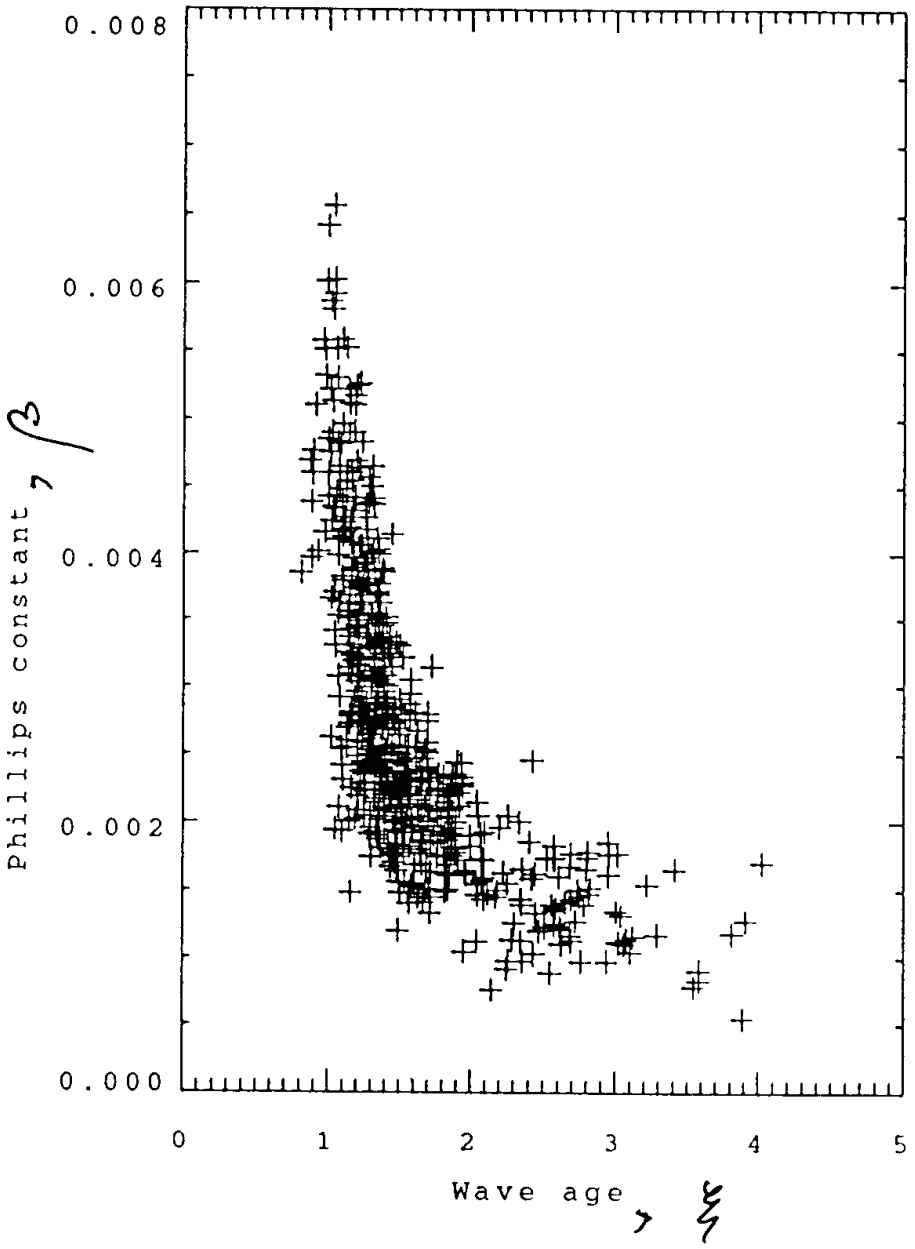
0.008
0.006
0.004
0.002
0.000
Phillips constant, β
0
1
2
3
4
5
Wave age, ξ

Fig. 9

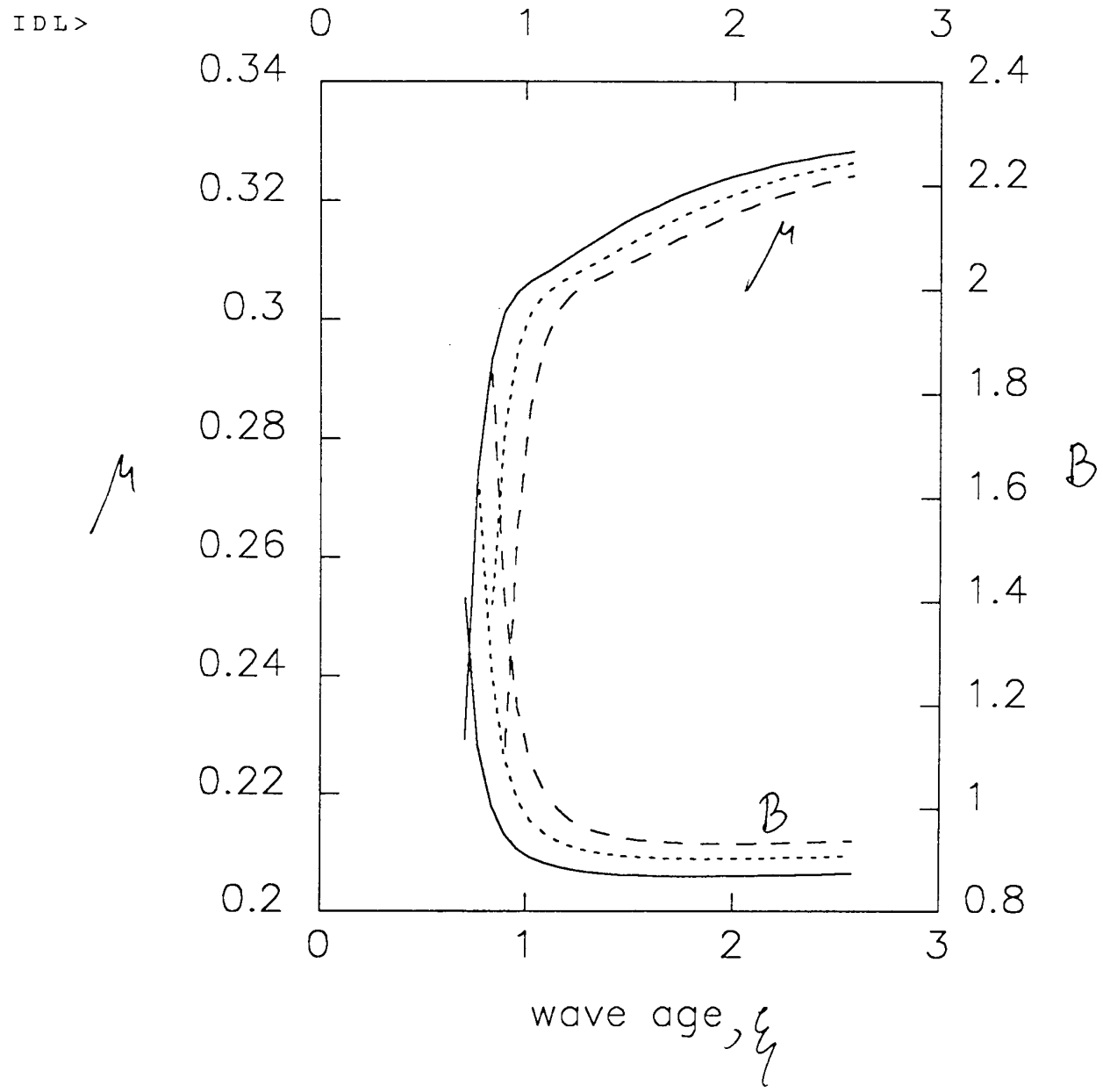
IDL>
0
1
2
3
0.34
0.32
0.3
0.28
0.26
0.24
0.22
0.2
2.4
2.2
2
1.8
1.6
1.4
1.2
1
0.8
μ
B
wave age, ξ

Fig. 10

IDL>

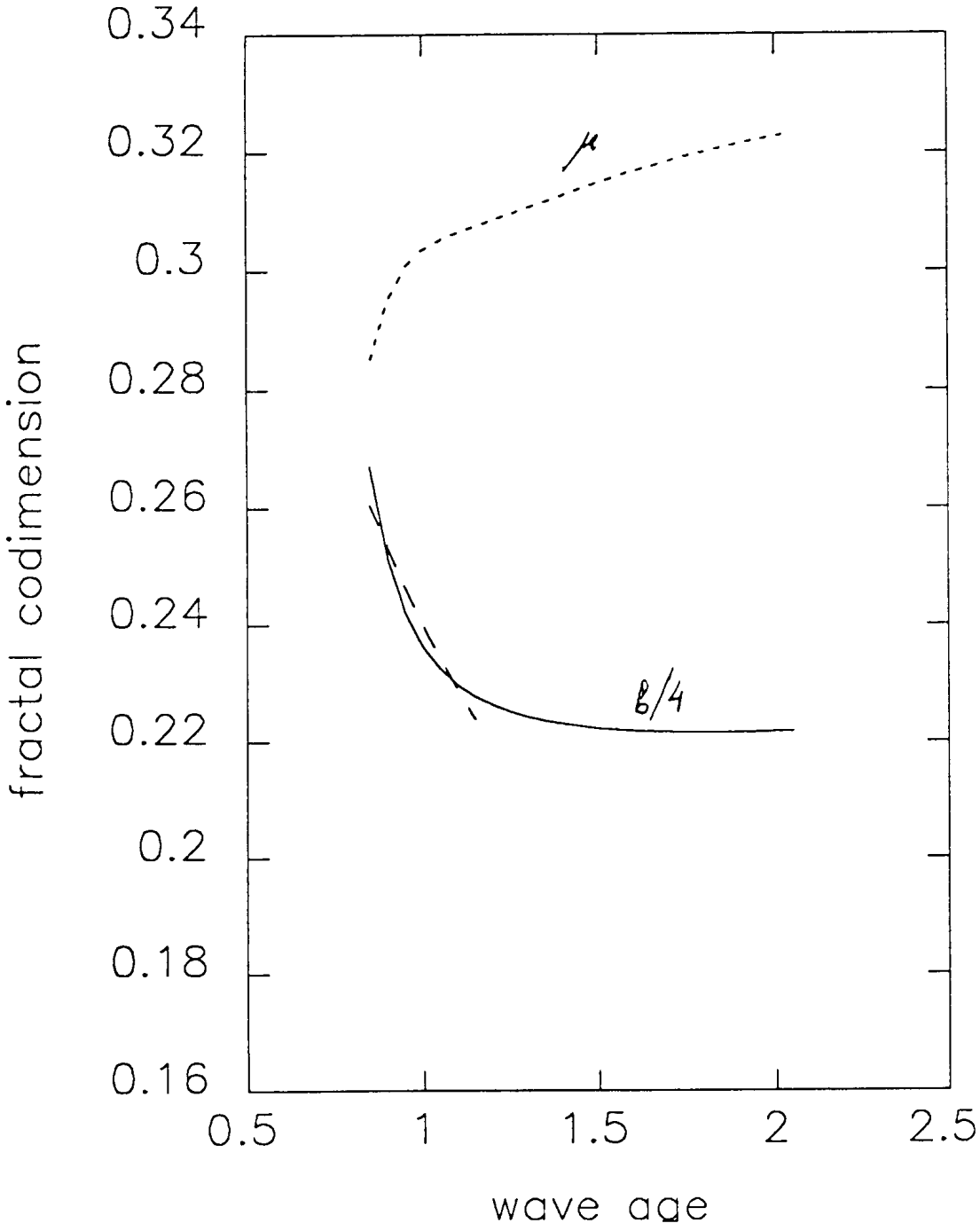
0.34
0.32
0.3
0.28
0.26
0.24
0.22
0.2
0.18
0.16
fractal codimension
0.5
1
1.5
2
2.5
wave age
μ
β/4

Fig. 11

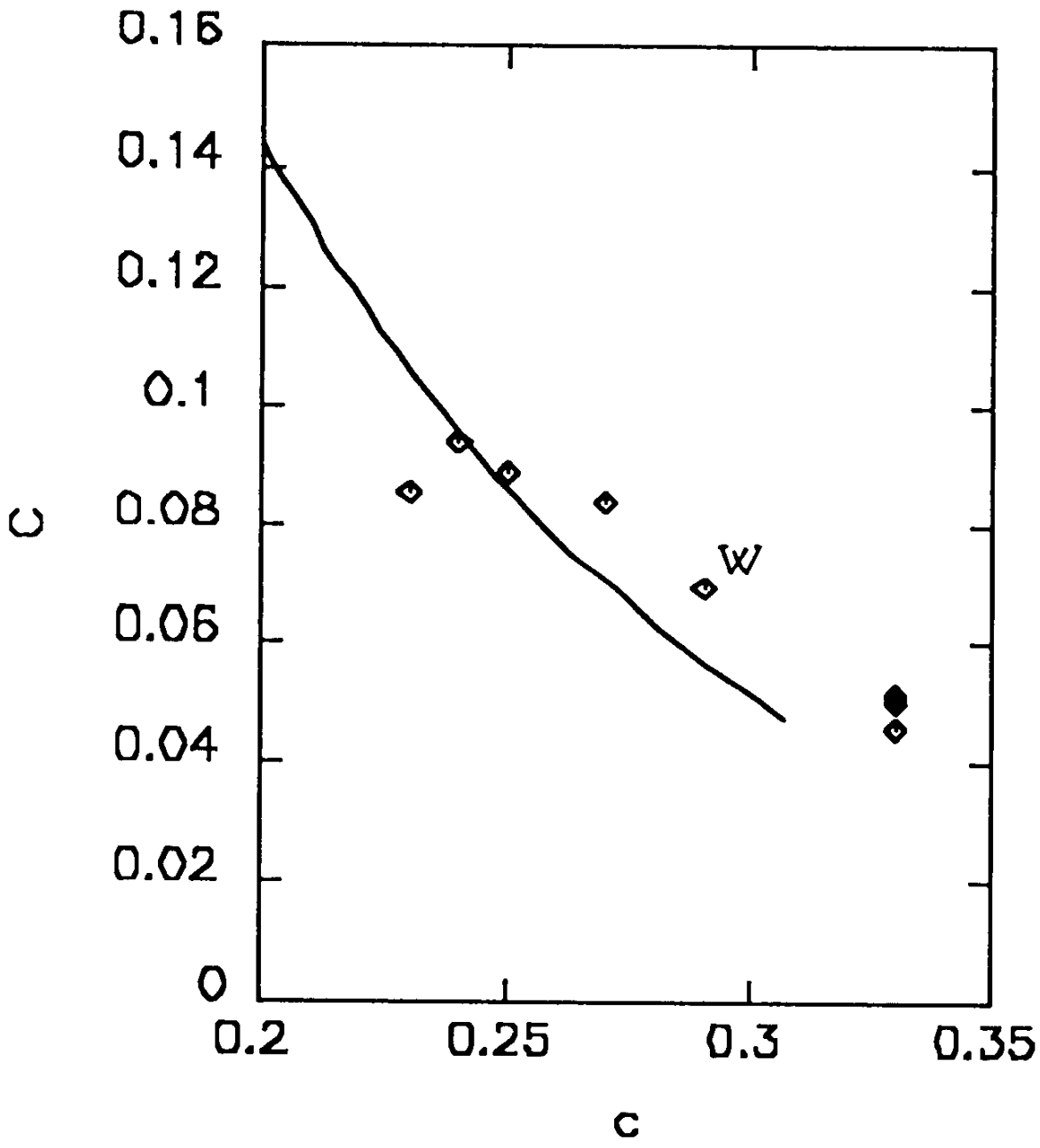

Fig. 12

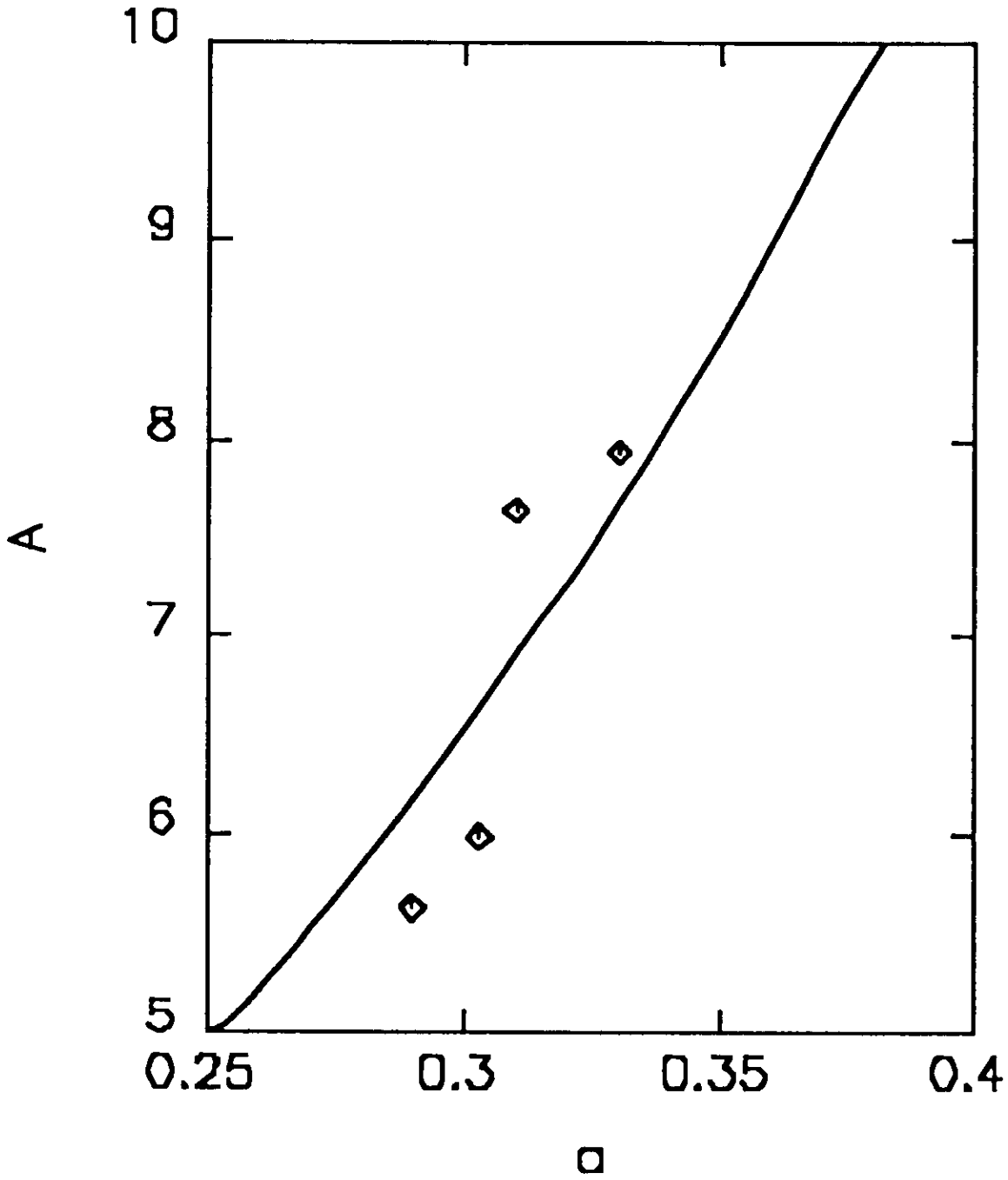

Fig. 13

$

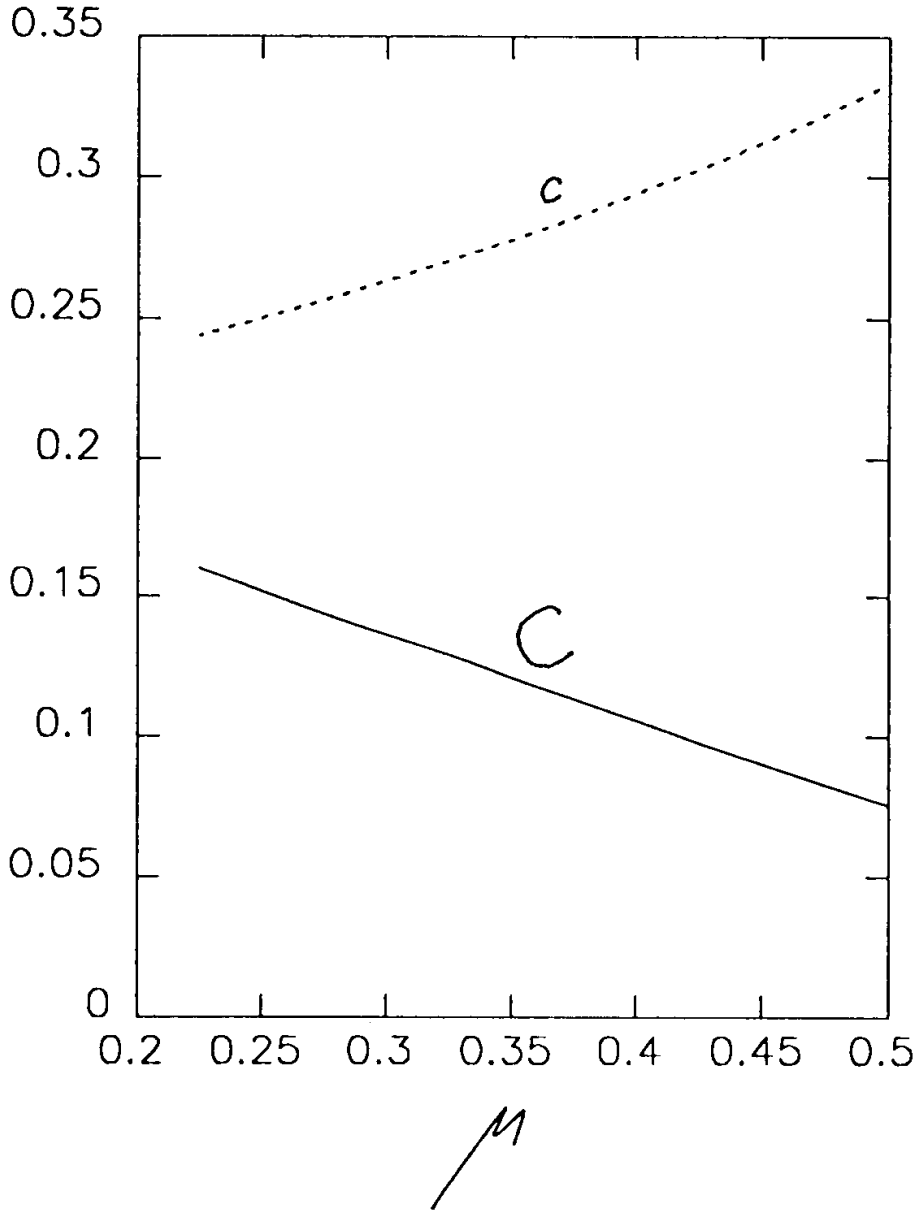

Fig #4